J. Chem. Sci. Vol. 127, No. 2, February 2015, pp. 225–233.
DOI 10.1007/s12039-015-0784-3

Interesting cationic ($Li^+/Fe^{3+}/Te^{6+}$) variations in new rocksalt ordered structures

AKANKSHA GUPTA, VINOD KUMAR and S UMA*
Materials Chemistry Group, Department of Chemistry, University of Delhi, Delhi 110 007, India
e-mail: suma@chemistry.du.ac.in

MS received 7 November 2014; accepted 12 November 2014

Abstract. A new series of layered oxides, $Li_3(Li_{1.5x}Fe_{3-(x+1.5x)}Te_x)O_6$, ($0.1 \leq x \leq 1.0$) possessing rocksalt superstructures crystallizing in monoclinic (S.G. *C2/m*) symmetry is reported here. Investigations based on single crystal and powder X-ray diffraction studies for the $x = 1$ member, $Li_3(Li_{1.5}Fe_{0.5}Te)O_6$, ($a = 5.1834(1)$; $b = 8.8858(2)$; $c = 5.16840(8)$ Å; $\beta = 110.660(1)°$) confirmed the stabilization of $(Li_{1.5}Fe_{0.5}Te_{1.0}O_6)^{3-}$ honeycomb arrays with a very high amount of lithium ions. The structure for the $x = 0.5$ member ($Li_{3.75}Fe_{1.75}Te_{0.5}O_6$) has also been confirmed by the powder X-ray diffraction Rietveld refinements. $Li_3(Li_{1.5}Fe_{0.5}Te)O_6$ and $Li_3(Li_{0.75}Fe_{1.75}Te_{0.5})O_6$ oxides exhibited Curie–Weiss behaviour in the temperature range of 50–300 K with negative θ values. Their respective ionic conductivities were found to be 6.76×10^{-5} S cm^{-1} and 2.21×10^{-6} S cm^{-1} at 573 K. The UV-visible diffuse reflectance measurements for the different members of the series $Li_3(Li_{1.5x}Fe_{3-(x+1.5x)}Te_x)O_6$, ($0.1 \leq x \leq 1.0$) show the expected shifts in their absorption edges based on the increasing amount of Fe^{3+} ions starting from $x = 1.0$ member to $x = 0.1$ member.

Keywords. Lithium-based oxides; rocksalt superstructures; single crystal XRD; honeycomb ordering; UV-visible diffuse reflectance.

1. Introduction

The layered oxides of the type AMO_2 (A = alkali metal ion; M = transition or post-transition metal ion) have been extensively studied by several researchers because of the wide range of compositions that can be obtained by various combinations of the A and M cations. The simplest members $LiCoO_2$ and $LiNiO_2$ are the popularly known cathode materials.[1,2] Structures of these oxides are derived from the rocksalt (NaCl) structure by the ordering of layers formed by the edge-shared (MO_6) octahedra separated by A^+ cations in various coordinations (figure 1). Different metal ion substitutions at the M site led to further ordered superstructures such as $Li_3M_2XO_6$ (M = Mg, Co, Ni, Cu; X = Nb, Ta, Bi, Sb) and $Na_3M_2XO_6$ (M = Mg Co, Ni, Cu, Zn; X = Sb).[3–11] The superstructures crystallizing mostly in space groups *P3$_1$12*, *C2/m* or *C2/c* arise from the additional ordering of the two M and one X ions, to form an ordered honeycomb array separated by interleaving Li^+ or Na^+ ions (figure 1). This particular arrangement of ions belong to the structure type named as O3 corresponding to the octahedral coordination (O) and the number of layers (3) found in the unit cell.[12] We recently reported the other examples Li_4MTeO_6 (M(II) = Co, Ni, Cu, Zn)[13] and Li_4MSbO_6 (M(III) = Cr, Fe, Al, Ga, Mn)[14] accompanied by independent reports on Li_4ZnTeO_6[15] and Li_4FeSbO_6[16] for O3 structure type. The Rietveld structural refinements of the powder X-ray diffraction (XRD) were carried out for most of the members of the above mentioned Te and Sb containing oxides and in few cases additional confirmation has been sought from single crystal XRD studies as well.[13,14] Among these oxides, Li_4NiTeO_6 has been reported as a potential cathode material for lithium ion batteries.[17] There exist another interesting series of oxides represented as $Na_2M_2TeO_6$ (M = Ni, Co, Zn, Mg) possessing P2 structures, nomenclature arising from their two-layer sequence in the unit cell with prismatic coordination of Na^+ ions in the interlayer region (figure 1).[18] They are excellent ionic conductors and crystallize in hexagonal space groups *P6$_3$22* or *P6$_3$/mcm*. The exceptions are $Na_2Cu_2TeO_6$ (S.G. *C2/m*) reported by Xu *et al*.[19] and its lithium analogue $Li_2Cu_2TeO_6$[20] obtained by us only via low temperature ion-exchange reaction. Two different polytypes I and II of $Li_2Ni_2TeO_6$ were also synthesized respectively by the low temperature ion-exchange reaction and by high temperature solid state method.[20]

*For correspondence

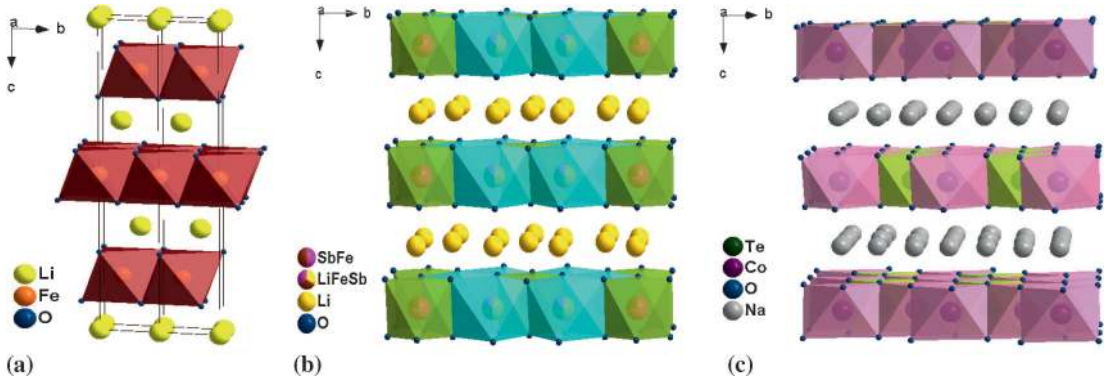

Figure 1. Crystal structures of **(a)** layered $LiFeO_2$ (O3 structure type, S.G.*R-3m*), **(b)** Li_4FeSbO_6 (O3 structure type, S.G. *C2/c*) and **(c)** $Na_2Co_2TeO_6$(P2 structure type, S.G. $P6_322$).

Among the rocksalt-based oxides, the Fe^{3+} containing metal oxides are specifically investigated to study the arrangement of Fe^{3+} (electronic configuration of d^5 in high spin) ions in the triangular network and also as possible cathode materials for lithium ion batteries. For example, Li_4FeSbO_6 containing magnetic $(LiFeSbO_6)^{3-}$ honeycomb arrays separated by non-magnetic Li^+ ions show antiferromagnetic order at $T_N \approx 3.6$ K.[16] During the investigation of the Na_2O–Fe_2O_3–Sb_2O_5 phase diagram, the corresponding sodium-containing Na_4FeSbO_6[21] has also been found to adopt a superstructure of the α-$NaFeO_2$ type based on the ordering of the $(NaFeSbO_6)^{3-}$ honeycomb slabs. Recently, Schmidt *et al.*[22] reported $Na_3LiFeSbO_6$ oxide with a similar rocksalt superstructure and showed that both Na_4FeSbO_6 and $Na_3LiFeSbO_6$ oxides exhibit Curie–Weiss behaviour consistent with the presence of high spin Fe^{3+}, but without any long range magnetic ordering. Reduction in the ratio of the interlayer Na^+ ions to the total number of cations in the honeycomb array (i.e., $(NaFeSbO_6)^{3-}$ or $((LiFeSbO_6)^{3-})$ of the mentioned oxides from 3:3 to 2:3 resulted in a different superstructure type. A tellurium-containing layered oxide $Na_2LiFeTeO_6$[23] crystallizing in $P2_12_12_1$ was synthesized and found to be related to the known P2 type $Na_2M_2TeO_6$ (Ni, Co, Zn, Mg) (S. G. $P6_3mcm$ or $P6_322$)[18] oxides. Our objective has been to explore the formation of new layered oxides specifically by arranging the $(LiFeTeO_6)^{3-}$ honeycomb layers with alternating Li^+ ions instead of Na^+ ions. In this process, we recognized that we could even vary the amounts of Li^+, Fe^{3+} and Te^{6+} ions in the honeycomb array and for the first time arrived at the series $Li_3(Li_{1.5x}Fe_{3-(x+1.5x)}Te_x)O_6$, $(0.1 \leq x \leq 1.0)$ of oxides. We report the synthesis and characterization of these new oxides with rocksalt superstructure and honeycomb ordering.

2. Experimental

Single crystals corresponding to the structure solution $Li_3(Li_{1.5}Fe_{0.5}Te_{1.0})O_6$ were initially obtained by heating a mixture of Li_2CO_3, Fe_2O_3, TeO_2 in the ratio of 3Li: 1Fe: 1Te, to a temperature of 1250°C followed by cooling to 1150°C at 2°C/h and then 1000°C at 5°C/h and finally cooled to 700°C at 10°C/h after which the furnace was switched off. Bulk polycrystalline samples for the obtained stoichiometry $Li_3(Li_{1.5}Fe_{0.5}Te_{1.0})O_6$ from the single crystal studies along with the other members of the series $Li_3(Li_{1.5x}Fe_{3-(x+1.5x)}Te_x)O_6$, $(0.1 \leq x < 1.0)$ were synthesized starting from high purity (Sigma Aldrich ≥99%) Li_2CO_3, Fe_2O_3 and TeO_2 by solid state method. Thoroughly homogenized stoichiometric quantities of the reactants were heated at 650°C for 12 h and finally at 900–950°C for 12–24 h.

2.1 *Characterization*

PXRD patterns were obtained using high resolution PANanalytical Empyrean diffractometer, consisting of pixel detector employing Cu K_α radiation ($\lambda = 1.5418$ Å) with a scan rate of 140 s/step and step size 0.013° at 298 K. The fitting of the PXRD patterns was carried out by LeBail method to obtain the unit cell parameters and the Rietveld refinement of the PXRD patterns of the $x = 1.00$ and 0.50 members were also carried out using GSAS+EXPGUI program.[24] SCXRD data for the $x = 1$ member was recorded on an Oxford Xcalibur NOVA diffractometer with a four circle κ goniometer employing a graphite-monochromatized Mo Kα ($\lambda = 0.71073$ Å) radiation at room temperature. The diffraction intensities were corrected for Lorentz polarization effects and the absorption corrections were carried out by multiple scan methods. The data were reduced using CrysAlisRED (available with the diffractometer). The structure was solved by direct methods and

refined using SHELXS 97[25] incorporated in WINGX suite.[26] UV−Visible diffuse reflectance data was collected in the spectral range 200−800 nm using Perkin-Elmer Lambda 35 scanning double beam spectrometer equipped with a 50 mm integrating sphere. $BaSO_4$ was used as a reference. For the estimation of the band gap, the data were transformed into absorbance using the Kubelka−Munk function. Sintered (at 900°C) pellets were used to measure the AC conductivity in the frequency range 1 to 10^7 Hz (Alpha N Analyzer Novocontrol, Pt electrode). The magnetic measurements were performed using a Quantum Design MPMS SQUID magnetometer under 1T magnetic field in the temperature range of 4–300 K. The oxidation state of tellurium in each of the members in the series $Li_3(Li_{1.5x}Fe_{3-(x+1.5x)}Te_x)O_6$, ($0.1 \leq x \leq 1.0$) of oxides were verified from redox titrations. Known quantities of the oxides were dissolved in 2M H_2SO_4, followed by the addition of 0.05M $FeSO_4$ solution. The resulting solution containing Te^{4+} produced by the reduction of Te^{6+}, along with the excess Fe^{2+}, was titrated with $KMnO_4$ solution.[18]

3. Results and Discussion

3.1 *Crystal structure*

PXRD pattern of the powder sample obtained by heating the reactants (Li_2CO_3, Fe_2O_3 and TeO_2) in the ratio of 3Li:1Fe:1Te indicated the formation of a monoclinic (S.G. *C2/m*) layered oxide resembling the PXRD patterns observed for the oxides Li_4MTeO_6 (Co, Ni, Cu, Zn)[13] and for Li_4FeSbO_6.[14,16] The single crystal growth and studies were attempted to ascertain the structure and stoichiometry according to the details given in the experimental and characterization sections. The SXRD data collected for an irregular plate-like brown coloured crystal confirmed the lattice parameters ($a = 5.1413(4)$, $b = 8.8424(5)$, $c = 5.1468(4)$ Å, $\beta = 110.395(8)°$) in a monoclinic symmetry (table S1). The systematic absences pointed towards a C–centred lattice with a possible *C2/m* space group. Structure solving by direct methods yielded the positions of the heavy atoms Te at *2a* and Fe at *4g* positions (table 1). The O atoms (at *4i* and *8j*) and the Li atoms (at *4h* and *2d*) were added subsequently from the electron density in the difference Fourier map. During the least square refinement cycles, occupancies of each one of the cationic sites were systematically verified to determine the cationic mixing while restraining the thermal and positional parameters. The refinement converged successfully ($R = 2.79\%$, $wR_2 = 4.67\%$, $GOF = 1.065$) for a structural model with Te1 in *2a*, Li1 in *4h* and a mixed Li2/Fe2 (0.97/0.03) at *2d* and Li3/Fe1(0.76/0.24) at the *4g* sites (table 1). The stoichiometry obtained was $Li_3(Li_{1.5}Fe_{0.5}Te)O_6$. The crystallographic parameters are listed in table S1 and the final positional and thermal parameters are listed in table 1 along with the anisotropic thermal parameters in table S2.

PXRD pattern of the polycrystalline oxide synthesized using the above stoichiometry $Li_{4.5}Fe_{0.5}TeO_6$ derived from the single crystal solution indeed confirmed the formation of a single phase (figure 2a). Rietveld refinement for the PXRD data was attempted and a structure similar to that from SXRD was obtained (table 1). The structure resembled that of Li_4FeSbO_6[16] and those of the various Li_4MTeO_6 (M = Co, Ni, Cu, Zn)[13] oxides, wherein the interlayer region was occupied only by Li^+ ions, separated by honeycomb layers formed by TeO_6 octahedra and $(Li/M)O_6$ octahedra. As compared to these mentioned oxides, in the present $Li_3(Li_{1.5}Fe_{0.5}Te)O_6$ oxide, the additional 0.5 lithium could be introduced at the cost of Fe^{3+} ions (present only in 0.5) leading to the formation of the honeycomb layers by the edge sharing of (TeO_6) octahedra, and $(Li3/Fe1)O_6$octahedra (figure 3). The structure has been noted with the formation of almost regular TeO_6 octahedra with Te–O bond lengths ranging between 1.914 and 1.929 Å. The bond lengths matched well with those reported earlier. These TeO_6 octahedra share edges with the $(Li3/Fe1)O_6$ octahedra whose bond lengths vary between 2.069 and 2.122 Å (table 2). The corresponding bond valence[27] values obtained from these bond distances matched well with those expected bond valences for Li^+, Fe^{3+} and Te^{6+} ions based on their oxidation states (table 2). The verification of occupancies in the Rietveld refinement of the PXRD pattern indicated the presence of only lithium ions (Li1 and Li2) in the interlayer region, as compared to the results from the SXRD refinements showing the presence of a small amount of iron (Fe2, 0.03) along with Li2 (0.97) (table 1). The Ag^+ ion-exchange experiments carried out using $Li_{4.5}Fe_{0.5}TeO_6$ with excess $AgNO_3$ around 250–300°C did not result in complete phase pure Ag^+ ion-exchanged product. Although, results from PXRD structural refinements indicated the presence of only Li^+ ions in the interlayer region (table 1), the results from ion-exchange reactions seemed to suggest the presence of a small amount of Fe^{3+} ions, thus coinciding with the SXRD refinement results. This behaviour is similar to that observed for Li_4CuTeO_6 oxide stabilized with a much higher amount (0.68) of Cu along with 0.32 of lithium at the *2d* site.[13] Thus, the exercise undertaken to determine the structure of $Li_{4.5}Fe_{0.5}TeO_6$ resulted in a stoichiometry possessing the highest amount of lithium

Table 1. Positional parameters, occupancies and thermal parameters of $Li_{4.5}Fe_{0.5}TeO_6$ from SXRD (bold) and PXRD measurements.

Atom	*Wyck*	*x/a*	*y/b*	*z/c*	SOF	U(iso)Å^2
Te1	***2a***	0	0	0	**1**	**0.0064(1)**
Te1	*2a*	0	0	0	1	0.0204(5)
Li1	***4h***	0	**0.1729(10)**	**0.5**	**1**	**0.017(1)**
Li1	*4h*	0	0.1945(16)	0.5	1	0.032(5)
Li2/Fe2	***2d***	**0.5**	**0**	**0.5**	**0.97/0.03**	**0.014(1)**
Li2	*2d*	0.5	0	0.5	1	0.025(7)
Li3/Fe1	***4g***	0	**0.3341(2)**	**0**	**0.76/0.24**	**0.0062(4)**
Li3/Fe1	*4g*	0	0.3284(4)	0	0.731(1)/0.269(1)	0.021(1)
O1	***4i***	**0.2303(7)**	**0**	**0.7772(7)**	**1**	**0.0105(7)**
O1	*4i*	0.2467(9)	0	0.7789(9)	1	0.016(1)
O2	***8j***	**0.2314(5)**	**0.1544(3)**	**0.2326(5)**	**1**	**0.0104(5)**
O2	*8j*	0.2232(6)	0.1530(2)	0.2380(7)	1	0.025(1)

ions, three in the interlayer region and 1.5 in the honeycomb array (i.e., $Li_3(Li_{1.5}Fe_{0.5}Te)O_6$) (figure 3). Li^+ with an octahedral ionic radius of 0.76 Å forms the octahedrally edge-shared honeycomb array with Te^{6+} (ionic radius (VI) = 0.56 Å) along with the different M^{2+} ions whose radii vary between 0.65 and 0.74 Å in the $Li_3(LiMTe)O_6$ (M + Co,Ni, Cu,Zn)[13]oxides and with Fe^{3+}(0.645Å) and Sb^{5+}(0.60 Å) in the related $Li_3(LiFeSb)O_6$ oxide.[14,16] Accordingly, based on the identification of $Li_3(Li_{1.5}Fe_{0.5}Te)O_6$, we considered the possibility of varying the amounts of Li^+, Fe^{3+} and Te^{6+} ions in the honeycomb array as well as the interlayer region leading to the series $Li_3(Li_{1.5x}Fe_{3-(x+1.5x)}Te_x)O_6$, $(0.1 \leq x \leq 1.0)$.

Formation of the remaining members belonging to the series $Li_3(Li_{1.5x}Fe_{3-(x+1.5x)}Te_x)O_6$, $0.1 \leq x \leq 0.75$ was verified by attempting the synthesis of polycrystalline samples. The PXRD patterns for the various members (x = 0.75, 0.67, 0.5, 0.33, 0.25 and 0.1) confirmed the formation of rocksalt-related structures similar to the x = 1.0 member. The refined lattice dimensions from the LeBail fit of the PXRD patterns (figure 2) are listed in table 3. The intensities of the superstructure reflections corresponding to the rocksalt superstructure in the $15^\circ \leq 2\theta \leq 25^\circ$ region systematically have been found to decrease (figure 2). Rietveld structural refinement was undertaken for the intermediate $x = 0.5$ member. The structure showed a clear distinction from the x = 1 member in the distribution of various Li^+/ Fe^{3+}/ Te^{6+} ions in the available crystallographic sites. Te^{6+} (Te1) and Fe^{3+}(Fe1) ions shared the *2a* site approximately with equal occupancies; and similarly, Li^+ (Li3) and Fe^{3+} (Fe3) ions occupy in equal amounts at the *4g* site. The remaining Fe^{3+} (Fe2) ions have been found to share the *2d* site with Li^+(Li2) ions to an extent of 0.78 and 0.22. Li^+ (Li1) ions alone occupy the *4h* site; thereby confirming the stoichiometry $Li_3(Li_{0.75}Fe_{1.75}Te_{0.5})O_6$ for the x = 0.5 member of the series, $Li_3(Li_{1.5x}Fe_{3-(x+1.5x)}Te_x)O_6$. Refinement results are listed in table 4 and the selected bond distances are given in table 5. The appropriate bond distances and corresponding bond valences that are derived reaffirm the structural model and the distribution of cations in the various crystallographic sites. Detailed structural refinements for the rest of the members of the series $Li_3(Li_{1.5x}Fe_{3-(x+1.5x)}Te_x)O_6$ are currently underway.

The coexistence of lithium ions segregated aptly in the interlayer region for ion-exchange reaction along with the M^{2+} and Te^{6+} ions in the honeycomb ordered array as found in the Li_4MTeO_6 (M(II) = Co, Ni, Cu, Zn)[13,15] oxides or with M^{3+} and Sb^{5+} ions as found in the Li_4MSbO_6 (M(III) = Cr, Fe, Al, Ga, Mn)[14,16] oxides serve as a prelude for the current series of oxides identified in this study. The surprisingly higher amount of incorporated lithium ions together with the continuous variation of all the three cations (Li^+, Fe^{3+}, Te^{6+}) are the additional significant features for studies involving lithium ion batteries and to identify analogous structural members with other suitable metal ions.

3.2 *Optical properties*

UV–Visible diffuse reflectance spectra were recorded for the different members belonging to the $Li_3(Li_{1.5x}Fe_{3-(x+1.5x)}Te_x)O_6$, $0.1 \leq x \leq 1.0$ series of oxides (figure 4). The diffuse reflectance data were converted to absorbance using Kubelka–Munk function.[28] The spectra clearly matched with the colour observed for the various members starting from x = 1.0 (buff colour) and all the members up to x = 0.1 (reddish brown). The resulting band gaps vary from 3.24 eV for

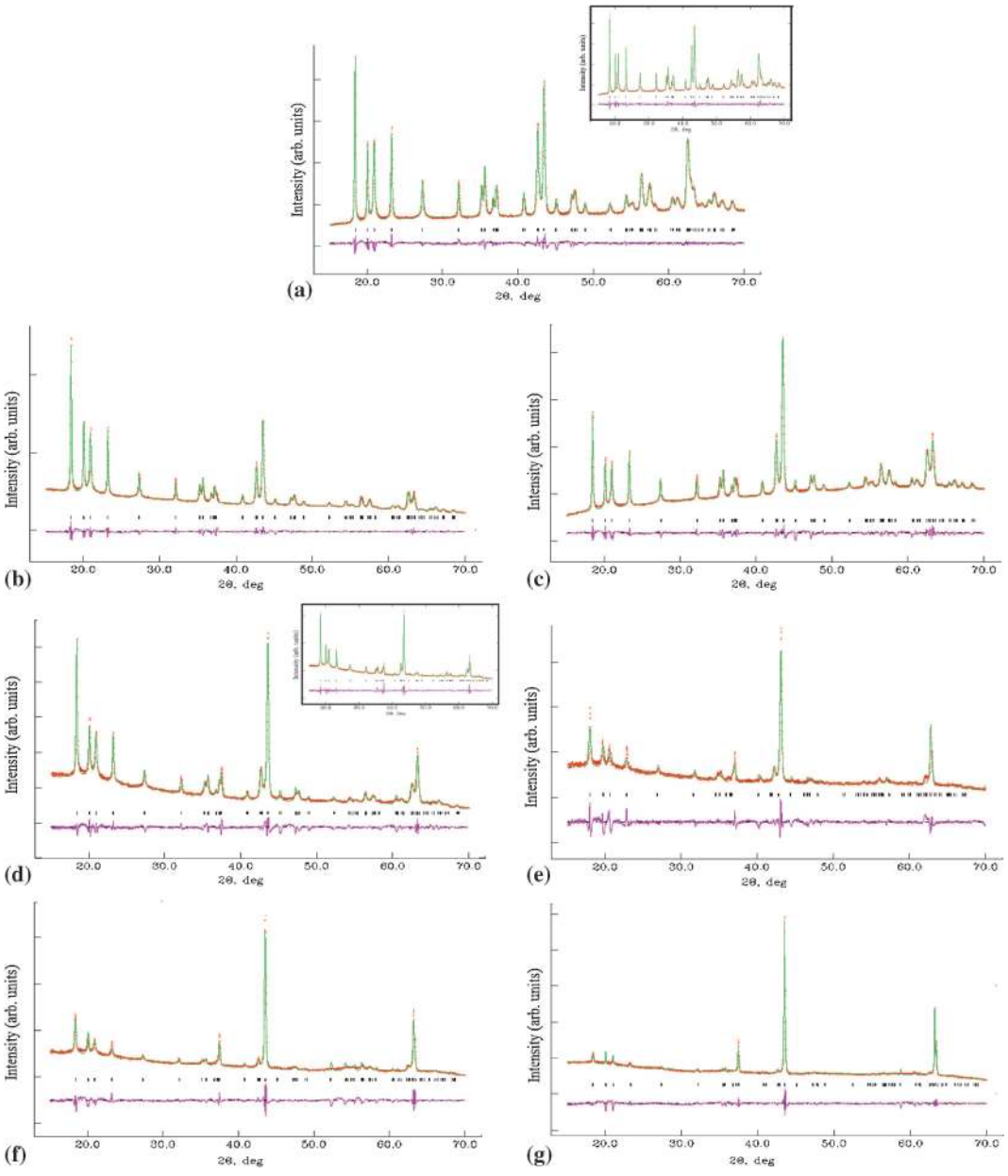

Figure 2. Full pattern fitting of PXRD patterns of $Li_3(Li_{1.5x}Fe_{(3-(x+1.5x)}Te_x)O_6$ for x = (**a**) 1.00, (**b**) 0.75, (**c**) 0.66, (**d**) 0.50, (**e**) 0.33, (**f**) 0.25 and (**g**) 0.10; red, experimental data; green line, calculated profile; pink line below, difference profile; vertical bars, Bragg positions. The corresponding Reitveld fittings are shown in the insets of (**a**) and (**d**).

$Li_{4.5}Fe_{0.5}TeO_6$ to 1.95 eV for $Li_{3.15}Fe_{2.75}Te_{0.1}O_6$. Particularly, the $x = 1$ member differs from the rest of $0.25 \leq x < 1.0$ members because of the increase in the amount of Fe^{3+} ions. Accordingly, the band gaps for these members do not differ much and range narrowly between 2.00 and 1.95 eV (figure 4).

3.3 *Magnetic susceptibility*

The DC magnetic susceptibility (χ_m) and the inverse susceptibility ($1/\chi_m$) with temperature plots are given for the $x = 1.0$ ($Li_{4.5}Fe_{0.5}TeO_6$) and $x = 0.5$ ($Li_{3.75}Fe_{1.75}Te_{0.5}O_6$) members of the series (figure 5). The respective Curie–Weiss fits yielded magnetic moments of 6.49 μ_B and 4.26 μ_B in the temperature range of 50–300 K as compared to the theoretical moment of 5.92 μ_B expected for Fe^{3+} (high spin $3d^5$). The negative Weiss constants of −20.32 K for $x = 1.0$ and −57.73 K for $x = 0.5$ suggested the presence of short range antiferromagnetic interactions.[22] However, no long range interactions were observed as seen in the case of Li_4FeSbO_6.[16] Detailed study of the magnetism with varying applied magnetic field and temperature for

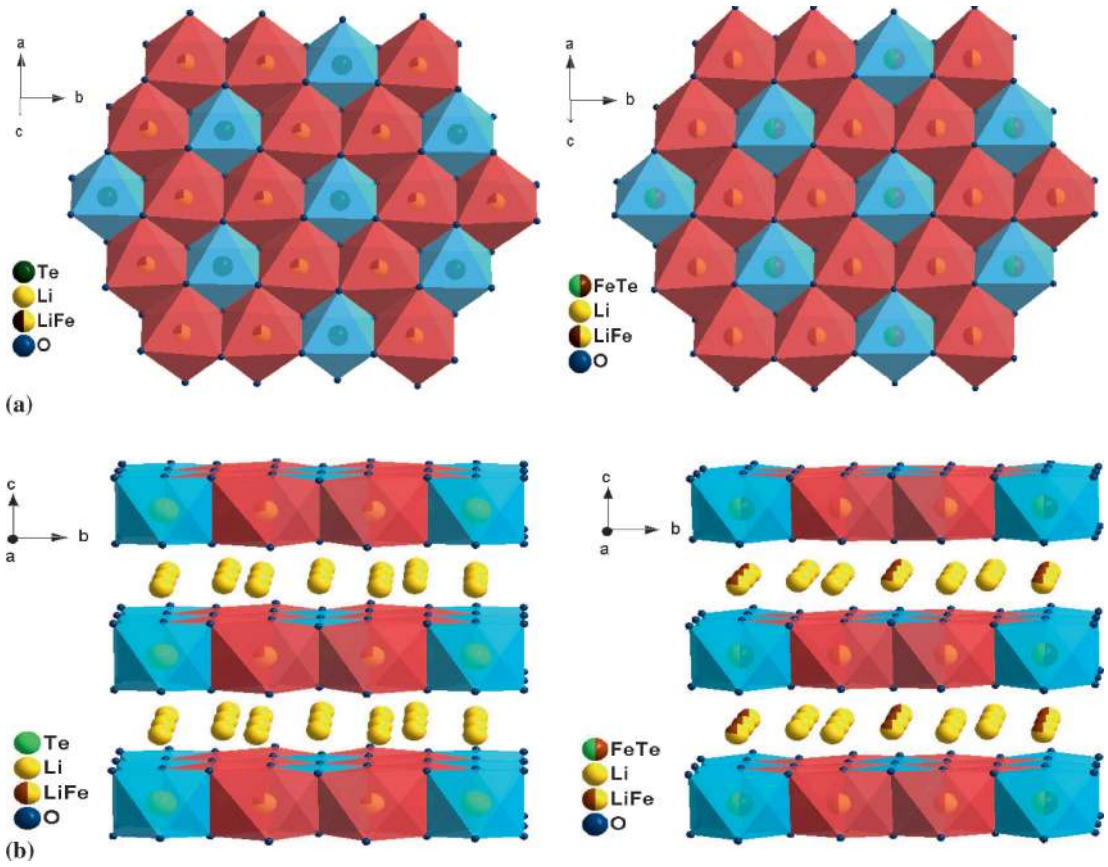

Figure 3. Structure of $Li_{4.5}Fe_{0.5}TeO_6$ and $Li_{3.75}Fe_{1.75}Te_{0.5}0_6$. (**a**) Honeycomb array of edge-shared MO_6 octahedra; (**b**) view perpendicular to the edge-shared honeycomb layers.

Table 2. Selected bond distances (in Å) of $Li_{4.5}Fe_{0.5}TeO_6$ from SXRD (bold) and PXRD measurements.

Bonds	Interatomic distances (Å)	Calculated* and observed BVS	Bonds	Interatomic distances (Å)	Calculated* and observed BVS
Te1— O1	**1.914(3) × 2**	**5.88* 6.0**	**Li2/Fe2— O1**	**2.310(3) × 2**	**0.99* 1.06**
Te1 – O1	1.99611(3)×2	5.45* 6.0	Li2 – O1	2.26359(4)× 2	0.96* 1.0
Te1— O2	**1.929(2) × 4**		**Li2/Fe2— O2**	**2.083(2) × 4**	
Te1 – O2	1.93239(3)× 4		Li2 – O2	2.09907(3)×4	
Li1— O1	**2.144(7) × 2**	**0.95* 1.0**	**Li3/Fe1— O1**	**2.069(3) × 2**	**1.41* 1.47**
Li1 – O1	2.32599(3) × 2	0.94* 1.0	Li3/Fe1 – O1	2.07204(3) × 2	1.40* 1.52
Li1— O2	**2.116(3) × 2**		**Li3/Fe1— O2**	**2.093(3) × 2**	
Li1 – O2	2.07698(3) × 2		Li3/Fe1 – O2	2.05703(3) × 2	
Li1— O2	**2.192(7) × 2**		**Li3/Fe1— O2**	**2.122(2) × 2**	
Li1 – O2	2.10075(3) × 2		Li3/Fe1 – O2	2.19807(4) × 2	

Table 3. Lattice parameters for the various members of the series $Li_3(Li_{1.5x}Fe_{3-(x+1.5x)}Te_x)O_6$ $(0.1 \leq x \leq 1.0)$.

Amount of x	a(Å)	b(Å)	c(Å)	β(°)	Volume(Å^3)
1.00	5.1834(1)	8.8858(2)	5.16840(8)	110.660(1)	222.742(5)
0.75	5.1643(1)	8.8397(1)	5.1516(1)	110.653(1)	220.063(6)
0.67	5.1560(1)	8.8295(1)	5.1360(1)	110.612(2)	218.855(2)
0.50	5.1686(2)	8.8362(3)	5.1508(3)	110.610(3)	220.19(1)
0.33	5.1848(4)	8.8331(4)	5.1429(3)	110.521(4)	220.59(2)
0.25	5.1718(5)	8.8442(1)	5.1473(6)	110.730(6)	220.197(2)
0.10	5.1245(2)	8.84182(6)	5.1627(5)	110.478(5)	219.14(2)

Table 4. Positional occupancies and thermal parameters for $Li_3(Li_{0.75}Fe_{1.75}Te_{0.5})O_6$.

Atom	*Wyck*	*x*/*a*	*y*/*b*	*z*/*c*	SOF	U(iso) Å^2
Te1/Fe1	*2a*	0	0	0	0.49(1)/0.51(1)	0.030(1)
Li1	*4h*	0	0.1877(27)	0.5	1	0.011(6)
Li2/Fe2	*2d*	0.5	0	0.5	0.778(4)/0.222(4)	0.020(4)
Li3/Fe3	*4g*	0	0.3255(4)	0	0.498(5)/0.498(5)	0.032(1)
O1	*4i*	0.2290(17)	0	0.7699(20)	1	0.019(2)
O2	*8j*	0.2260(11)	0.1639(3)	0.2143(10)	1	0.023(2)

Table 5. Selected bond distances (in Å) of $Li_{3.75}Fe_{1.75}Te_{0.5}O_6$.

Bonds	Interatomic distances (Å)	Calculated* and observed BVS
Te1/Fe1— O1	1.94149(6) × 4	4.59* 4.47
Te1/Fe1— O2	1.94836(8) × 2	
Li1— O1	2.10289(8) × 4	0.98* 1.00
Li1— O1	2.18814(10) × 2	
Li1— O2	2.21850(7) × 2	
Li2/Fe2— O1	2.19264(8) × 4	1.55* 1.44
Li2/Fe2— O2	2.29399(10) × 2	
Li3/Fe3— O1	1.92678(6) × 2	2.03* 1.99
Li3/Fe3— O2	2.08130(9) × 2	
Li3/Fe3— O2	2.14090(7) × 2	

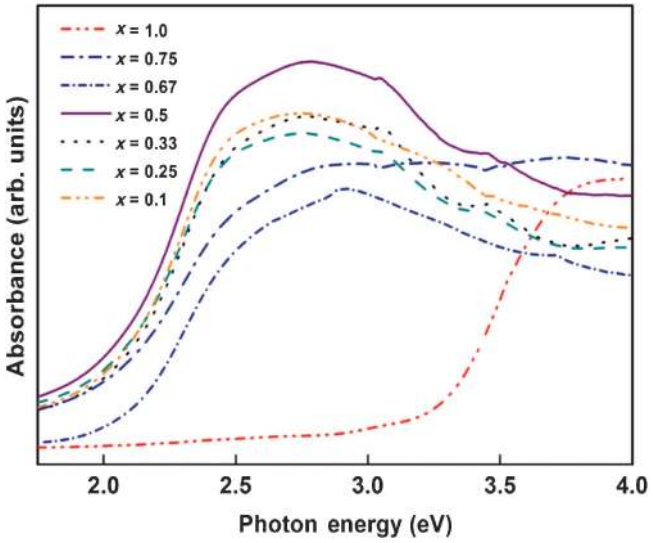

Figure 4. UV–Visible diffuse reflectance spectra data converted to absorbance vs. eV for the various members of the series $Li_3(Li_{1.5x}Fe_{(3-(x+1.5x)}Te_x)O_6$ ($0.1 \leq x \leq 1.0$).

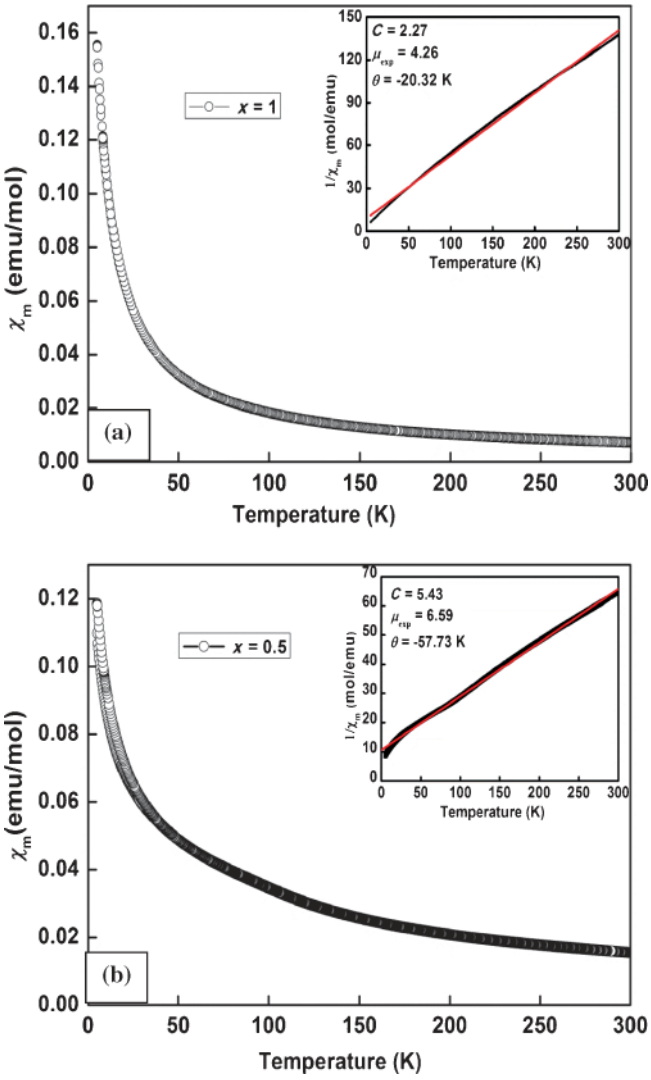

Figure 5. Temperature dependence of magnetic susceptibility at H = 1T for $Li_3(Li_{1.5x}Fe_{(3-(x+1.5x)}Te_x)O_6$ (**a**) $x = 1.0$ and (**b**) $x = 0.5$. Insets show the respective plots of inverse susceptibility with temperature.

all the members in the current series may provide further information on the interactions of the Fe^{3+} ions in the honeycomb array as well as the additional interactions arising from a Fe^{3+} ions present with the Li^+ ions in the interlayer region. It may also provide a reason for the observed deviation in the magnetic moments for the $x = 1$ and 0.5 members.

3.4 *Ionic conductivity*

Ion-exchange behaviour for the present series of oxides seemes to be limited because of the shared occupancy of Li^+ ions with Fe^{3+} ions in the interlayer region. However, ionic mobilities were checked by measuring their conductivities. Activation energies

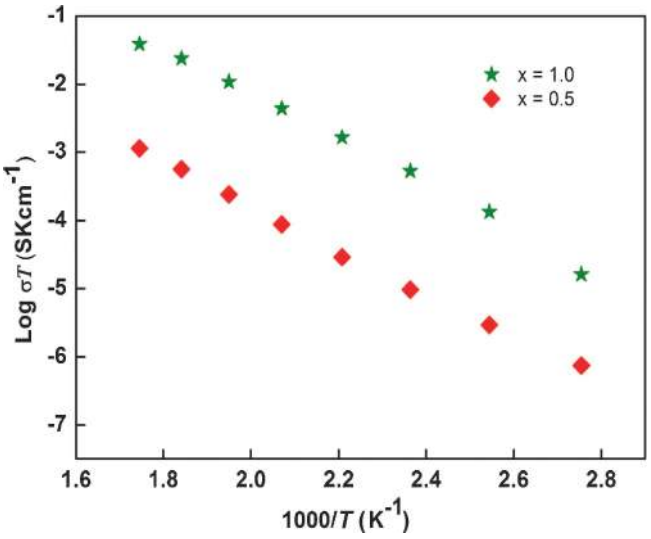

Figure 6. Arrhenius ionic conductivity plots of $Li_3(Li_{1.5x}Fe_{(3-(x+1.5x)}Te_x)O_6$ for (**a**) $x = 1.0$ and (**b**) $x = 0.5$ for total (ac) conductivity.

were calculated using the relation $\sigma_{DC} = \sigma_o \exp(-\Delta E_a/k_B T)$, where E_a is the activation energy, k_B is the Boltzmann's constant and σ_o is pre-exponent factor. Conductivity values at 573 K for the $x = 1.0$ and $x = 0.5$ members were 6.76×10^{-5} S cm^{-1} and 2.21×10^{-6} S cm^{-1}, respectively (figure 6). The respective activation energies were found to be 0.70(4) and 0.60(1) eV. Contribution from the electronic conductivities could be considered particularly at higher temperatures.

4. Conclusions

The variation of Li^+, Fe^{3+} and Te^{6+} ions based on appropriate charge balancing resulted in new rocksalt superstructure series of oxides $Li_3(Li_{1.5x}Fe_{3-(x+1.5x)}Te_x)O_6$ ($0.1 \leq x \leq 1.0$) for the first time. Detailed structural investigation by SXRD and PXRD studies for the $x = 1.0$ member and PXRD for the $x = 0.5$ member confirmed the extent of cationic mixing in the honeycomb array and also in the interlayer. Preliminary magnetic susceptibility measurements suggested Curie–Weiss behaviour for these $Li_{4.5}Fe_{0.5}Te_{1.0}O_6$ and $Li_{3.75}Fe_{1.75}Te_{0.5}O_6$ members in the range of 50–300 K with negative θ values. The diffuse reflectance measurements showed systematic shifts in their absorption edges from $x = 1.0$ to 0.1 members consistent with the colour arising from the increasing amount of Fe^{3+} ions. Ionic mobility based on the conductivity and activation energies was found to be nominal for the $Li_{4.5}Fe_{0.5}Te_{1.0}O_6$ and $Li_{3.75}Fe_{1.75}Te_{0.5}O_6$ oxides. Incorporation of additional lithium ions along with a red–ox-type Fe^{3+} metal ion to yield oxides with rocksalt superstructure is significant specially for the electrode material aspects of lithium ion battery research.

Supplementary Information

Tables S1 – S3 are given as supplementary information. For details, see www.ias.ac.in/chemsci.

Acknowledgements

This work was supported by the DST (SR/S1/PC-07/2011), DST – Nanomission, Government of India and University of Delhi under the 'Scheme to Strengthen R & D Doctoral Research Program'. We thank the USIC, Delhi University for the SXRD facilities. VK thanks CSIR and AG thanks DST, Government of India for fellowships.

References

1. (a) Whittingham M S 2008 *MRS Bull.* **33** 411; (b) Goodenough J B and Kim Y 2010 *Chem. Mater.* **22** 587; (c) Huggins R A 2009 *Advanced batteries: Materials science aspects* (New York: Springer)
2. Whittingham M S 2004 *Chem. Rev.* **104** 4271
3. Greaves C and Katib S M A 1990 *Mat. Res. Bull.* **25** 1175
4. Mather G C, Smith R I, Skakle J M S, Fletcher J G, Castellanos R M A, Gutierrez M P and West A R 1995 *J. Mater. Chem.* **5(8)** 1177
5. Mather G C and West A R 1996 *J. Solid State Chem.* **124** 214
6. Skakle J M S, Castellanos R M A, Tovar S T and West A R 1997 *J. Solid State Chem.* **131** 115
7. Smirnova O A, NalbandyanV B, Petrenko A A and Avdeev M 2005 *J. Solid State Chem.* **178** 1165
8. Viciu L, Huang Q, Morosan E, Zandbergen H W, Greenbaum, N I, McQueen T and Cava R J 2007 *J. Solid State Chem.* **180** 1060
9. Politaev V V, Nalbandyan V B, Petrenko A A, Shukaev I L, Volotchaev V A and Medvedev B S 2010 *J. Solid State Chem.* **183** 684
10. Zvereva E A, Evstigneeva M A, Nalbandyan V B, Savelieva O A, Ibragimov S A, Volkova O S, Medvedeva L I, Vasiliev A N, Klingeler R and Buechner B 2012 *Dalton Trans.* **41** 572
11. (a) Berthelot R, Schmidt W, Muir S, Eilertsen J, Etienne L, Sleight A W and Subramanian M A 2012 *Inorg. Chem.* **51** 5377 (b) Seibel E M, Roudebush J H, Wu H, Huang Q, Ali M N, Ji H and Cava R J 2013 *Inorg. Chem.* **52** 13605
12. Delmas C, Fouassier C and Hagenmuller P 1980 *Physica* **99B** 81
13. Kumar V, Bhardwaj N, Tomar N, Thakral V and Uma S 2012 *Inorg. Chem.* **51** 10471
14. Bhardwaj N, Gupta A and Uma S 2014 *Dalton Trans.* **43** 12050
15. Nalbandyan V B, Avdeev M and Evstigneeva M A 2013 *J. Solid State Chem.* **199** 62

16. Zvereva E A, Savelieva O A, Titov Y D, Evstigneeva M A, Nalbandyan V B, Kao C N, Lin J-Y, Presniakov I A, Sobolev A V, Ibragimov S A, Hafiez M A, Krupskaya Y, Jähne C, Tan G, Klingeler R, Büchner B and Vasilieva A. N. 2013 *Dalton Trans.* **42** 1550
17. Sathiya M, Ramesha K, Rousse G, Foix D, Gonbeau D, Guruprakash K, Prakash A S, Doublet M L and Tarascon J-M 2012 *Chem. Commun*. 1
18. Evstigneeva M A, Nalbandyan V B, Petrenko A A, Medvedev B S and Kataev A A 2011 *Chem. Mater*. **23** 1174
19. Xu J, Assoud A, Soheilnia N, Derakhshan S, Cuthbert H L, Greedan J E, Whangbo M H, and Kleinke H 2005 *Inorg. Chem*. **44** 5042
20. Kumar V, Gupta A and Uma S 2013 *Dalton Trans.* **42** 14992
21. Politaev V V and Nalbandyan V B 2009 *Solid State Sci.* **11** 144
22. Schmidt W, Berthelot R, Etienne L, Wattiaux A and Subramanian M A 2014 *Mater. Res. Bull*. **50** 292
23. Nalbandyan V B, Petrenko A A and Evstigneeva M A 2013 *Solid State Ionics* **233** 7
24. (a) Larson A C and VonDreele R B 2004 *General Structure Analysis System (GSAS)*, Los. Alamos National Laboratory Report LAUR 86-748 (b) Toby B H 2001 *J. Appl. Cryst.* **34** 210
25. Sheldrick G M 1997 SHELXL97, *Programs for crystal structure analysis* (Germany: University of Gottingen)
26. FarrugiaL J 1999 *J. Appl. Crystallogr.* **32** 837
27. (a) Brown I D 2002 *The chemical bond in inorganic chemistry, the bond valence model* (Oxford: Oxford University Press); (b) Brown I D 2009 *Chem. Rev.* **109** 6858 (c) Brown I D 1992 *Z. Kristallogr*. **199** 255
28. (a) Kubelka P and Munk F 1931 *Z. Tech. Phys. (Leipzig)* **12** 593; (b) Kubelka P 1948 *J. Opt. Soc. Am.* **38** 448; (c) Yang L and Kruse B 2004 *J. Opt. Soc. Am.* **21** 1933